

1 **Structure and function of the ROR2 cysteine-rich domain in vertebrate noncanonical WNT5A**  
2 **signaling**

3  
4 Samuel C. Griffiths<sup>1†</sup>, Jia Tan<sup>2†</sup>, Armin Wagner<sup>3</sup>, Levi Blazer<sup>4</sup>, Jarret J. Adams<sup>4</sup>, Sachdev S. Sidhu<sup>4</sup>,  
5 Christian Siebold<sup>1\*</sup>, Hsin-Yi Henry Ho<sup>2\*</sup>

6  
7 <sup>1</sup>Division of Structural Biology, Wellcome Centre for Human Genetics, University of Oxford,  
8 United Kingdom

9 <sup>2</sup>Department of Cell Biology and Human Anatomy, University of California, Davis, United States

10 <sup>3</sup>Science Division, Diamond Light Source, Harwell Science and Innovation Campus, Didcot,  
11 United Kingdom

12 <sup>4</sup>The Donnelly Centre, University of Toronto, Canada

13

14

15

16 †co-first authors

17 \*co-corresponding authors

18

19

20 **Abstract**

21 The receptor tyrosine kinase ROR2 mediates noncanonical WNT5A signaling to orchestrate tissue  
22 morphogenetic processes, and dysfunction of the pathway causes Robinow syndrome,  
23 Brachydactyly B and metastatic diseases. The domain(s) and mechanisms required for ROR2  
24 function, however, remain unclear. We solved the crystal structure of the extracellular cysteine-  
25 rich (CRD) and Kringle (Kr) domains of ROR2 and found that, unlike other CRDs, the ROR2 CRD  
26 lacks the signature hydrophobic pocket that binds lipids/lipid-modified proteins, such as WNTs,  
27 suggesting a novel mechanism of receptor action. Functionally, we showed that the ROR2 CRD,  
28 but not other domains, is required and minimally sufficient to promote WNT5A signaling, and  
29 Robinow mutations in the CRD and the adjacent Kr alter ROR2 function. Moreover, we  
30 demonstrated that the activity of the ROR2 CRD requires Frizzled receptors. Thus, ROR2 acts via  
31 its CRD to potentiate the function of a receptor supercomplex that includes Frizzleds to transduce  
32 WNT5A signals.

## 33 **Introduction**

34 ROR proteins make up an important branch of the receptor tyrosine kinase (RTK) superfamily,  
35 conserved from sponges to humans. Originally identified as orphan receptors based on sequence  
36 homology to other RTKs (hence the name Receptor tyrosine kinase-like Orphan Receptor), work  
37 over the past two decades has elucidated a critical role of the ROR RTK family in mediating  
38 noncanonical WNT5A signaling (Oishi et al., 2003, Mikels and Nusse, 2006, Ho et al., 2012, Green  
39 et al., 2008). Unlike canonical WNTs, which signal through  $\beta$ -catenin-dependent transcription to  
40 regulate cell proliferation and tissue fate, WNT5A signals noncanonically through  $\beta$ -catenin-  
41 independent mechanisms to induce cytoskeletal rearrangements and tissue morphogenetic  
42 changes (Veeman et al., 2003, Moon et al., 1993). The pathway is also of clinical significance, as  
43 mutations in WNT5A, the ROR family member ROR2, and the downstream signal transducers  
44 DISHEVELLED 1 (DVL1) and DVL3 have been reported to cause Robinow syndrome (RS), a  
45 congenital disorder characterized by systemic tissue shortening defects, including dwarfism,  
46 mesomelic limb shortening, brachydactyly, genitourinary defects, cleft palate and other  
47 craniofacial dysmorphisms (Person et al., 2010, Afzal et al., 2000, van Bokhoven et al., 2000, Bunn  
48 et al., 2015, White et al., 2015, White et al., 2016). A distinct cohort of ROR2 missense mutations  
49 cause brachydactyly type B (BDB) (Oldridge et al., 2000, Schwabe et al., 2000). Moreover,  
50 elevated expression of ROR1 or ROR2 correlates with increased cancer metastatic potentials, and  
51 several anti-ROR therapies are currently in various stages of development (Rebagay et al., 2012).  
52 The etiological mechanisms of these mutations, however, remain largely uncharacterized. Thus,  
53 a greater understanding of ROR receptor function is important from both basic science and  
54 medical perspectives.

55 ROR receptors are type-I transmembrane proteins with a single-pass transmembrane  
56 (TM) helix linking extracellular and intracellular regions. The extracellular region of vertebrate  
57 ROR proteins contains an immunoglobulin (Ig) domain, a Frizzled-like cysteine rich domain (CRD)  
58 and a Kringle domain (Kr). The intracellular region includes a tyrosine kinase domain (Tk), a  
59 proline-rich domain (PRD), and two serine/threonine-rich domains (S/TRD 1 and 2) (Minami et  
60 al., 2010, Green et al., 2008). The specific requirement of these domains in WNT5A signaling  
61 remains controversial. Early genetic studies in *C. elegans* showed that only the CRD and the TM  
62 helix are essential for the function of the nematode ROR homolog Cam-1 in cell migration, which  
63 raised the possibility that Cam-1 may not act as a typical RTK and may instead regulate the spatial  
64 distribution of WNT ligands (Kim and Forrester, 2003). Experiments in vertebrate systems,  
65 however, largely suggest that ROR proteins act as bone fide signaling receptors and that this  
66 function requires other domains of ROR proteins, including the intracellular domains (DeChiara  
67 et al., 2000, Mikels et al., 2009). However, due to the historical lack of tractable assays to directly  
68 measure ROR activity, the precise requirement of vertebrate ROR proteins in noncanonical  
69 WNT5A signaling has not been systematically examined.

70 The CRD is of broader interest because it is not only conserved within the ROR family but  
71 also among other important receptor classes where the domain mediates ligand and/or co-factor  
72 binding through a signature hydrophobic groove or pocket (Bazan and de Sauvage, 2009). For  
73 instance, the CRD of the classical WNT receptor Frizzled interacts with the palmitoleate moiety  
74 of WNT ligands directly through this groove (Janda et al., 2012). Free fatty acids have also been  
75 observed to interact in the same fashion (Nile et al., 2017). Moreover, the CRD of the Hedgehog  
76 signal transducer and GPCR Smoothed (Smo) binds cholesterol through an analogous

77 hydrophobic pocket (Byrne et al., 2016). Because the CRD of ROR2 was previously implicated in  
78 WNT5A binding (Oishi et al., 2003), and shares a high degree of amino acid sequence similarity  
79 with the Frizzled CRD (Xu and Nusse, 1998, Saldanha et al., 1998), it is assumed that it possesses  
80 a similar hydrophobic groove via which it interacts with WNT5A. However, this hypothesis  
81 remains untested, as both the requirement of ROR2 CRD in WNT5A signaling and its atomic  
82 structure have not been determined.

83         In this study, we determined the crystal structure of the ROR2 CRD and Kr domains.  
84 Remarkably, we found that the two domains share an extended interface and that the ROR2 CRD  
85 lacks the characteristic hydrophobic groove/pocket for interacting with lipids. The latter  
86 observation suggests that the ROR2 CRD cannot mediate high-affinity interaction with the  
87 palmitoleate group of WNT5A. To further probe the requirement of the ROR2 CRD in WNT5A  
88 signaling, we developed a functional complementation assay in ROR1/ROR2 double knockout  
89 mouse embryonic fibroblasts (MEFs) and showed that the ROR2 CRD is required and minimally  
90 sufficient to mediate WNT5A-ROR signaling. Moreover, we used this assay paradigm to  
91 demonstrate that several Robinow patient mutations in the CRD and Kr domains compromise  
92 WNT5A-ROR signaling and offered structural insights into their possible underlying molecular  
93 defects. Lastly, using a highly specific monoclonal antibody that blocks Frizzled receptor activity,  
94 we established that the Frizzled family is required for the ability of the ROR2-CRD to mediate  
95 WNT5A signaling. Collectively, the study provides structural and functional insights into ROR2  
96 function, and supports a model in which ROR2 functions through its CRD to promote Frizzled-  
97 dependent WNT5A signaling.

98



## 99 **Results**

### 100 **The structure of the ROR2 CRD and Kr domains**

101 To determine the structure of the ROR2 CRD, we expressed a range of constructs  
102 comprising the full-length human ROR2 extracellular region (Fig. 1A). Analysis of construct  
103 secretion revealed that deletion of the Kr domain severely impacted the yield of ROR2 constructs  
104 (Fig. S1A), and therefore the full extracellular region (ECD) and CRD-Kr were selected for large-  
105 scale expression and purification (Fig. S1B and C).

106 We determined a crystal structure of the ROR2 CRD-Kr tandem domain construct at a  
107 resolution of 2.7 Å via a platinum single-wavelength anomalous dispersion experiment coupled  
108 with molecular-replacement (MR-SAD) (Table S1, Fig. S1D-F; see experimental procedures for  
109 details). The CRD comprises 5  $\alpha$ -helices ( $\alpha$ 1-5) and a single  $\beta$ -sheet (strands  $\beta$ 1 and  $\beta$ 2), while the  
110 Kr domain presents a characteristic lack of secondary structure, displaying a single  $\beta$ -sheet  
111 (strands  $\beta$ 3 and  $\beta$ 4) (Fig. 1B, left-hand panel). The CRD is stabilized by 5 disulfide bonds: one  
112 located between  $\beta$ 1 and a loop extending from helix  $\alpha$ 2 (I), a second linking  $\alpha$ 2 and the loop  
113 preceding longest helix  $\alpha$ 1 (II), a third between helix  $\alpha$ 2 and the loop between helices  $\alpha$ 3/4 (III),  
114 a fourth between long loops following helices  $\alpha$ 2 and  $\alpha$ 3 (IV), and the fifth between helix  $\alpha$ 3 itself  
115 and the loop extending from  $\alpha$ 5 (V). The Kr domain is stabilized by 3 disulfide bonds, the first of  
116 which (VI) is formed between the very N-terminus and the C-terminus of the domain. Two  
117 additional disulfide bonds (VII and VIII) are found within the core of the Kr domain.

118 Overall, the CRD and Kr domains form an associated structural unit (Fig. 1B, right-hand  
119 panel). A contact interface is observed between the two domains and is dominated by van der  
120 Waals interactions, with a single hydrogen bond present (Fig. 1C). The domains share a small

121 interfacial area of 354 Å<sup>2</sup>, with a reasonable shape complementarity score (0.7) (Lawrence and  
122 Colman, 1993). Kr domains are generally observed to constitute protein-protein interfaces within  
123 multi-domain proteins (Deguchi et al., 1997, Ultsch et al., 1998, Zebisch et al., 2016), suggesting  
124 that the ROR2 Kr domain acts to stabilize the CRD (Fig. S1A).

125         The full-length ROR2 ECD is monomeric in solution at concentrations as high as 48 μM  
126 (Fig. S1B and C), indicating that the CRD does not mediate dimerization as has been suggested  
127 for other related Frizzled-type CRDs (Dann et al., 2001). The CRD-Kr structural unit arrangement  
128 observed in the crystal structure is conserved in solution, confirmed by small-angle X-ray  
129 scattering (SAXS) experiments (Fig. S2A-D), with the N-terminal Ig domain connected by a flexible  
130 linker (Fig. S2C). Structurally, the ROR2 CRD is evolutionarily related to other Frizzled-type  
131 ‘groove-containing’ CRDs (Nachtergaele et al., 2013), such as MuSK and Fz8 (Fig. 1D and Table  
132 S2) (Stiegler et al., 2009, Dann et al., 2001, Janda et al., 2012), as well as the cholesterol-binding  
133 Hedgehog signal transducer Smo (Byrne et al., 2016). These are structurally distinct to the  
134 ‘pocket-type’ CRDs such as NPC1 and RFBP, which bury their physiological ligands in deep cavities  
135 (Bazan and de Sauvage, 2009).

136

### 137 **Structural analysis of ROR2 CRD function**

138 The Frizzled-type CRDs from both Fz8 and Smo exhibit shallow hydrophobic grooves for the  
139 binding of palmitoleate or cholesterol, respectively (Janda et al., 2012, Byrne et al., 2016) (Fig. 2).  
140 One general characteristic differentiating this sub-family of CRDs from the ‘pocket-type’ sub-  
141 family is that these grooves are structurally conserved when ligand-free (Fig. 2A and B), with  
142 minimal structural rearrangements upon ligand binding (Dann et al., 2001, Janda et al., 2012,

143 Nachtergaele et al., 2013, Byrne et al., 2016). Despite structural conservation with other Frizzled-  
144 type receptors, the ROR2 CRD does not contain a visible hydrophobic groove pre-formed for  
145 ligand recognition (Fig. 2D). A structure-based sequence alignment shows that the ROR2 CRD has  
146 evolved an additional helical insertion ( $\alpha 5$ ) relative to the FZD8 CRD (Fig. 2E). Structural  
147 superposition of the ROR2 CRD with the Fz8:Wnt-palmitoleate binary complex (Janda et al., 2012)  
148 shows that this helical insertion blocks exposure of any possible palmitoleate-binding groove (Fig.  
149 2F and G). This observation is therefore incompatible with a direct binding event occurring  
150 between the ROR2 CRD and the WNT5A palmitoleate moiety, suggesting that the high affinity  
151 'site 1' WNT5A interaction must occur either via a different site on the CRD or through a separate  
152 co-receptor(s), or require structural rearrangements as-yet not observed for groove-containing  
153 Fz-CRDs.

154

### 155 **Functional requirement of the ROR2 CRD in WNT5A signaling**

156 We next examined the requirement of the ROR2 CRD, as well as that of other ROR2 domains, in  
157 WNT5A signaling. We first developed a central rescue paradigm that allowed us to exogenously  
158 express various ROR2 mutant proteins in *ROR1/ROR2* double knockout (ROR DKO) mouse  
159 embryonic fibroblasts (MEFs) and assess their ability to restore WNT5A signaling (Fig. 3A). We  
160 isolated E12.5 primary MEFs from *ROR1/ROR2* double conditional mutant embryos for these  
161 experiments, as we previously showed that MEFs from this embryonic age are highly responsive  
162 to WNT5A-ROR signaling (Susman et al., 2017). To enable long-term genetic manipulations, we  
163 immortalized the MEFs (called iMEFs) via Cas9/CRISPR-mediated ablation of the *Tp53* gene (Dirac  
164 and Bernards, 2003). We then treated the iMEFs with 4-hydroxy-tamoxifen, which activates the

165 genetically encoded Cre-ER protein, to induce deletion of the *ROR1* and *ROR2* genes. To allow  
166 quantitative measurement of WNT5A-ROR signaling, we further engineered a GFP-Pdzrn3  
167 degradation reporter construct into the iMEFs. We previously reported that activation of WNT5A-  
168 ROR signaling induces the proteasomal degradation of downstream effector protein Pdzrn3, and  
169 that this regulation could be recapitulated using the GFP-Pdzrn3 reporter in live cells via flow  
170 cytometry (Konopelski, 2021). Lastly, to compare the activities of wildtype (WT) ROR2 versus its  
171 mutant derivatives, we developed a lentivirus-based gene replacement strategy that allowed the  
172 expression of ROR2 “rescue” constructs at near-endogenous levels (See Materials and Methods  
173 for details). WNT5A dose-response analysis comparing ROR DKO reporter cells versus WT ROR2  
174 rescued cells showed that re-expression of WT ROR2 promoted WNT5A signaling across all  
175 WNT5A doses tested (Fig. 3B). Notably, ROR DKO reporter cells without any ROR2 rescue still  
176 retained some basal WNT5A signaling activity, which remains dose-dependent with respect to  
177 WNT5A concentration (Fig. 3B). This observation indicates that, while ROR receptors play an  
178 impotent role in promoting WNT5A signaling, additional receptor(s) exist in these cells to  
179 transmit the WNT5A signal.

180 To systematically identify the domain(s) of ROR2 required for WNT5A signaling, we used  
181 our structural information to generate a series of ROR2 domain truncation mutants (Fig. 3C) and  
182 assessed their ability to restore WNT5A signaling in our iMEF signaling rescue assay (Fig. 3E).  
183 Immunoblotting confirmed that the mutant proteins were expressed at comparable levels as WT  
184 ROR2 (Fig. 3D). WNT5A stimulation experiments showed that ROR2 mutants lacking the CRD  
185 ( $\Delta$ CRD and  $\Delta$ CRD-Kr) failed to restore WNT5A-induced degradation of the GFP-Pdzrn3 reporter  
186 (Fig. 3E), establishing that the CRD is essential for WNT5A signaling. Surprisingly, all other

187 mutants in the series, including one lacking almost the entire intracellular region, still retain  
188 significant signaling capability, indicating that only the CRD is indispensable for the core function  
189 of ROR2 in promoting WNT5A signaling (Fig. 3E).

190 We next assessed the sufficiency of the ROR2 CRD in mediating WNT5A signaling. We  
191 engineered a chimeric construct (mini-ROR2) in which the isolated ROR2 CRD is fused to a generic  
192 transmembrane helix from CD45 (Chin et al., 2005), followed by a small, intracellular  
193 juxtamembrane fragment (Fig. 3C). Expression of mini-ROR2 in the ROR DKO iMEF reporter cells  
194 was sufficient to partially rescue WNT5A signaling (Fig. 3E). This experiment, taken together with  
195 the truncation analysis, established that the ROR2-CRD is required and minimally sufficient to  
196 support the function of ROR2 in WNT5A signaling.

197

### 198 **Co-requirement of Frizzled receptors in WNT5A-ROR signaling**

199 Based on the observations that ROR DKO iMEFs still retain some signaling activity (Fig. 3B), and  
200 that ROR lacking the intracellular region can still function (Fig 3E), we postulated that ROR  
201 proteins cannot by themselves function as the signaling receptors for WNT5A; instead, they most  
202 likely facilitate the signaling function of another receptor(s). Members of the Frizzled family are  
203 likely candidates, as they are known to interact with WNT5A directly (Sato et al., 2010, Oishi et  
204 al., 2003) and have been implicated in aspects of WNT5A/ROR signaling (Grumolato et al., 2010,  
205 Oishi et al., 2003), and overexpression of Frizzleds can mimic the effect of WNT5A on Pdzrn3  
206 degradation (Konopelski, 2021). To directly test the requirement of Frizzleds in WNT5A signaling,  
207 we treated our iMEF reporter cells with a synthetic monoclonal antibody, F2.A, that binds the  
208 CRD of many Frizzled family members and inhibits its ability to interact with WNTs (Pavlovic et

209 al., 2018). Indeed, this treatment completely blocked WNT5A-dependent degradation of the GFP-  
210 Pdzrn3 reporter in either ROR DKO iMEFs or ROR DKO iMEFs rescued with WT ROR2 (Fig. 3F).  
211 Thus, Frizzled receptors are required for WNT5A to signal the degradation of Pdzrn3, likely as  
212 part of a co-receptor complex with RORs (Fig. 3G).

213

#### 214 **Robinow syndrome mutations in the ROR2 CRD and Kr domains compromise WNT5A signaling**

215 Of all the ROR2 domains, the CRD and Kr domains are most frequently mutated in Robinow  
216 syndrome patients (Tufan et al., 2005, Afzal et al., 2000, Tamhankar et al., 2014, Mehawej et al.,  
217 2012). Our structural and functional data suggest that these mutations would disrupt the  
218 function of ROR2 in WNT5A signaling. To test this hypothesis, we expressed and characterized  
219 five substitution mutations from Robinow patients that map to the CRD (C182Y, R184C, R189W,  
220 C223Y, R272C) and two that map to the Kr domain (G326A and R366W), using the ROR DKO iMEF  
221 rescue system. Western blot analysis showed that all seven mutant proteins were expressed at  
222 comparable levels as WT ROR2 (Fig. 4A). In WNT5A signaling assays, we found that three of the  
223 five CRD mutations (C182Y, R184C and C223Y) and both Kr mutations (G326A and R366W)  
224 exhibited significantly reduced signaling capabilities (Fig. 4B). These results indicate that  
225 disruption of ROR2 CRD/Kr function by these mutations is the likely molecular cause of Robinow  
226 syndrome.

227 Further insights into the pathogenic mechanisms of Robinow mutations were obtained  
228 from our structural analysis. C182Y and C223Y disrupt conserved cysteines in the CRD. Since our  
229 structure showed that all 10 cysteines in the CRD are involved in disulfide bond formation (Fig.  
230 1B), these mutations likely cause Robinow syndrome by destabilizing the core structure of the

231 CRD (Fig. 4C, 4D and 4E). Two other mutations in the CRD (R184C and R272C) involve amino acid  
232 substitution to cysteines. Since both of these residues are solvent exposed (Fig. 4C, 4D and 4E),  
233 they may form cryptic intramolecular disulfide bonds that disrupt the protein fold, or  
234 alternatively form intermolecular disulfide bonds that cause inappropriate dimerization or  
235 oligomerization that results in protein aggregation. R189W and R272C did not show obvious  
236 functional deficit in our assay system. As the severity of Robinow syndrome can vary among  
237 individual patients and mutations, it is possible that more subtle defects are not detected by our  
238 system, or that they are involved in other aspects of ROR2 regulation beyond Pdzrn3 degradation.

239         Interestingly, the most detrimental mutations in the series (G326A and R366W) both map  
240 to the Kr domain at locations near the CRD-Kr interface (Fig. 4C and 4F). G326 in particular is  
241 situated near the linker between the CRD and Kr (Fig. 4C and 4C), and therefore, substitution at  
242 this position may open up the space between the two domains and expose hydrophobic residues  
243 to promote protein aggregation. Likewise, R366W may disrupt the overall fold of Kr, or disrupt  
244 the interface between the CRD and Kr to destabilize the CRD-Kr structural unit (Fig. 4C and 4C).  
245 Together, these functional and structural analyses provide crucial insights into the molecular  
246 mechanisms of Robinow pathogenesis.

247

## 248 **Discussion**

249 In this study, we used an integrated approach of structural biology, genetics and pharmacology  
250 to better understand the mechanism of WNT5A signal reception at the cell surface. We made  
251 several key observations that substantially advance our current understanding of WNT5A  
252 receptor function.

253 First, by solving the crystal structure of the ROR2 CRD, we made the surprising finding  
254 that this domain lacks the characteristic hydrophobic groove that binds the acyl moiety of WNTs  
255 and is thus incompatible with high affinity interaction with WNT ligands. Our experimental data  
256 agree with the modeling work by Janda and Garcia, who also predicted that the ROR2 CRD might  
257 not possess the hydrophobic groove to accommodate the lipid modification of WNTs (Janda and  
258 Garcia, 2015). This also agrees with the published crystal structure of MuSK, which is related to  
259 ROR2 and also lacks the hydrophobic groove in its CRD (Stiegler et al., 2009). The occlusion of the  
260 lipid/small molecule-binding site in ROR2 is unexpected and of general interest because this site  
261 was previously shown to play an important role not only for Wnt-Frizzled binding and Frizzled  
262 dimerization during canonical WNT signaling, but also for SMO function during Hedgehog  
263 signaling (Janda et al., 2012, Byrne et al., 2016, Nachtergaele et al., 2013, Nile et al., 2017). As  
264 there is clear evidence that the mammalian WNT5A is lipidated (Mikels and Nusse, 2006), our  
265 data raised the question of which co-receptor(s) in the pathway, if not ROR, is responsible for  
266 high-affinity WNT5A binding and signal transduction across the membrane. Though the exact  
267 identity of this co-receptor remains to be determined, our work points to the Frizzled receptor  
268 family, as blocking Frizzled function using a highly-specific and validated antibody blocked  
269 WNT5A signaling. We therefore favor a model in which WNT5A interacts with Frizzled with high  
270 affinity to transduce its signal across the plasma membrane, either by itself or in conjunction with  
271 another yet unidentified protein. However, this model does not rule out the possible presence  
272 of a low-affinity WNT5A binding site in the ROR2 CRD, analogous to the low affinity “site 2”  
273 observed in the WNT8-FZ8 complex (Janda et al., 2012). The ROR2 CRD could possibly sensitize  
274 WNT5A signaling by stabilizing the binding interaction between WNT5A and Frizzled via the



275 formation of a Frizzled:WNT:ROR2 super-complex (Fig. 3G). In this scenario, the WNT5A  
276 palmitoleate modification engages the Frizzled groove as previously described ('site 1')(Janda et  
277 al., 2012), whilst ROR2 binds at site 2 to recruit intracellular effectors of noncanonical WNT  
278 signaling. It is also possible that ROR2 acts by inducing an allosteric change in the structure of  
279 Frizzled to enhance Frizzled function or promotes Frizzled dimerization that in turn increases  
280 Frizzled's affinity for WNT5A (Carron et al., 2003, Nile et al., 2017).

281         Second, we observed that ROR2 mutants lacking the intracellular domain ( $\Delta$ ICD and mini-  
282 ROR2) can still support WNT5A signaling. This is inline with the idea that ROR2 itself is unlikely to  
283 be the signal-transmitting receptor for WNT5A. This idea is further supported by our observation  
284 that some residual signaling activity persists in cells lacking both ROR1 and ROR2 when stimulated  
285 with exogenously added WNT5A; we also show that this residual signaling activity is Frizzled-  
286 dependent. Collectively, these findings firmly established a co-requirement for both ROR and  
287 Frizzled activities in noncanonical WNT5A signal transduction. This model is also consistent with  
288 previous *in vivo* work showing that *ROR1/ROR2* double knockout mice phenocopy the  
289 characteristic tissue truncation phenotypes of *WNT5A* KO mice, and that human mutations in  
290 *WNT5A*, *ROR2* and *FZD2* can all cause Robinow syndrome with similar structural abnormalities  
291 (Nagasaki et al., 2018, White et al., 2018, Person et al., 2010, Afzal et al., 2000). Though several  
292 previous co-immunoprecipitation experiments have shown binding interactions between  
293 WNT5A and ROR2 (Oishi et al., 2003, Mikels and Nusse, 2006), between WNT5A and Frizzled  
294 family members (Sato et al., 2010), and between Frizzled and ROR proteins (Oishi et al., 2003), it  
295 remains unclear whether any of these biochemical interactions are direct. In light of our present  
296 work, it is crucial to further define these interactions quantitatively in future studies and to

297 understand their functions in the context of a co-receptor supercomplex. Nonetheless, our  
298 results showing that ROR2 acts through its CRD to sensitize the function of Frizzleds or a Frizzled-  
299 containing receptor complex during WNT5A-ROR signaling form the foundation for future  
300 studies.

301       Lastly, our work provided new insights into the molecular mechanisms of Robinow  
302 pathogenesis. Using the gene replacement strategy in iMEFs, we were able to directly assay the  
303 function of Robinow syndrome mutant variants under highly physiological conditions. We found  
304 that nearly all of the mutants tested exhibited defects in mediating WNT5A signaling, and that  
305 mutating the cysteines required for disulfide bonds in the CRD is not tolerated. Furthermore, by  
306 combining these functional data with our structural analysis, we can classify the mutations based  
307 on their locations on the CRD-Kr structure and infer potential underlying mechanisms of signaling  
308 perturbation. We envision that the experimental approach described in this study will serve as  
309 an important model for interrogating other mutations in the pathway that cause Robinow  
310 syndrome, brachydactyly type B and cancer metastasis, and more generally as a paradigm for  
311 modeling genetic disorders.

312

313

314

315

316  
317

**Supplementary Table 1. Data collection and refinement statistics for ROR2 CRD-Kr**

	<b>ROR2 CRD-Kr (Native)</b>	<b>ROR2 CRD-Kr (Pt-SAD)</b>	<b>ROR2-CRD-Kr (S-SAD)</b>
<b>Data collection</b>			
Beamline	DLS-I03	DLS-I03	DLS-I23
Space group	P3 <sub>2</sub> 21	P3 <sub>1</sub> 21	P3 <sub>1</sub> 21
Unit-cell parameters a, b, c (Å) $\alpha$ , $\beta$ , $\gamma$ (°)	109.6, 109.6, 45.0 90.0, 90.0, 120.0	106.1, 106.1, 42.2 90.0, 90.0, 120.0	113.6, 113.6, 45.1 90.0, 90.0, 120.0
No. of crystals / data sets	1/1	2/2	1/1
Wavelength (Å)	0.9763	1.0500	1.7711
Resolution (Å)	54.80-2.70 (2.75-2.70)	53.00-3.00 (3.10-3.00)	56.80-2.95 (3.03-2.95)
No. of unique reflections	8699 (443)	5599 (397)	7171 (519)
Completeness (%)	99.4 (100.0)	99.9 (99.5)	98.6 (96.5)
Multiplicity	9.9 (8.7)	28.1 (24.3)	184.7 (38.7)
$\langle I/\sigma(I) \rangle$	16.3 (1.0)	23.5 (6.4)	25.0 (1.6)
R <sub>merge</sub> (%)	7.8 (>100)	14.7 (59.6)	44.2 (>100)
R <sub>pim</sub> (%)	2.6 (8.3)	3.0 (12.3)	3.2 (33.5)
CC <sub>1/2</sub>	1.0 (0.5)	1.0 (0.8)	1.0 (0.9)
<b>Refinement</b>			
No. reflections (test set)	8688 (430)	-	
R <sub>work</sub> /R <sub>free</sub>	24.2 / 25.6	-	
No. atoms			
Protein	1670	-	
Ligand	10	-	
Mean B factor (Å <sup>2</sup> )			
Protein	112.0	-	
Ligand	137.1	-	
RMSD bond lengths (Å)	0.008	-	
RMSD bond angles (Å)	0.91	-	
Ramachandran plot (%)			
Favoured	96.1	-	
Allowed	3.4	-	
Outliers	0.5	-	

318

319 Data in parenthesis refer to highest resolution shell unless otherwise stated. RMSD: Root Mean  
320 Square Derivative.  
321

322  
323

**Supplementary Table 2. Evolutionary analysis of CRD structures.**

Protein	Fz8-PAM (4FOA) <sup>A</sup>	Smo (5L7D)	Fz8 (1IJY)	sFRP3 (1IJX)	MuSK (3HKL)	NPC1 (3GKI)	RFBP (not in PDB)	FR $\alpha$ (4LRH)	JUNO (5EJN)	FR $\beta$ (4KMZ)
ROR2	1.19 <sup>B</sup> 81 <sup>C</sup> 39.62 <sup>D</sup>	1.3078 35.87	1.3083 37.19	1.2883 36.53	0.88110 62.08	1.9474 27.99	2.4058 17.20	2.5054 15.39	2.4350 15.10	2.3851 15.57
Fz8-PAM (4FOA)		1.0083 43.64	0.16117 102.54	0.42106 79.01	1.3078 38.33	2.1761 21.36	2.5440 13.35	2.7644 12.16	2.5144 13.31	2.4443 14.14
Smo (5L7D)			1.0984 43.18	1.0480 44.60	1.2678 40.84	2.3254 19.01	2.6846 11.24	2.6246 13.73	2.6444 12.47	2.4948 15.65
Fz8 (1IJY)				0.45108 78.07	1.3576 36.13	2.1462 22.27	2.5045 15.00	2.6643 13.41	2.3845 15.40	2.5343 14.34
sFRP3 (1IJX)					1.3679 36.65	2.4160 17.28	2.3145 17.60	2.5947 14.13	2.4939 13.87	2.4746 15.62
MuSK (3HKL)						2.1467 22.48	2.2555 20.03	2.3055 15.14	2.1653 19.21	2.1353 23.24
NPC1 (3GKI)							1.7382 35.46	1.9589 31.57	1.7481 36.37	1.7490 30.58
RFBP (not in PDB)								0.68160 104.06	0.85138 80.30	0.66157 105.39
FR $\alpha$ (4LRH)									0.42161 125.21	0.16194 176.05

<b>JUNO (5EJN)</b>										0.46 157 120.8 3
------------------------	--	--	--	--	--	--	--	--	--	---------------------------

324

325 <sup>A</sup>PDB accession codes displayed in parenthesis; <sup>B</sup>RMSD values were calculated for equivalent C $\alpha$   
326 atom positions using the program SHP (Riffel et al., 2002; Stuart et al., 1979); <sup>C</sup>Number of  
327 equivalent C $\alpha$  positions used in calculation of RMSD values with SHP; <sup>D</sup>Summed structural  
328 correlation (total probability) values calculated via SHP. The phylogenetic tree for CRDs analyzed  
329 (Fig. 1C) was assembled using PHYLIP (Felsenstein, 1989). These summed structural correlation  
330 values were used to construct a distance matrix. Fz8-PAM – Frizzled 8-palmitoleate complex  
331 (Janda et al., 2012), Smo – Smoothened (Byrne et al., 2016), Fz8 – Frizzled 8 (Dann et al., 2001),  
332 sFRP3 – secreted Frizzled-related protein 3 (Dann et al., 2001), MuSK – muscle-specific kinase  
333 (Stiegler et al., 2009), NPC1 – Niemann-Pick C1 protein (Kwon et al., 2009), RFBP – riboflavin-  
334 binding protein (Monaco, 1997), FR $\alpha$  – folate receptor  $\alpha$  (Chen et al., 2013), FR $\beta$  – folate receptor  
335  $\beta$  (Wibowo et al., 2013), JUNO – folate receptor  $\delta$  (Han et al., 2016). Fz7 – Frizzled 7, Fz7-C24 –  
336 Frizzled 7-C24 fatty acid complex (Nile et al, 2017).

337

338

## 339 **Methods**

340 **Protein expression and purification.** Constructs of Human ROR2 (Genbank ID: 19743898)  
341 comprising the ECD (residues 34-403), Ig-CRD (60-307), CRD-Kr (171-396) and CRD (171-307)  
342 were cloned into the pHLsec vector in frame with a C-terminal His<sub>6</sub>-tag (Aricescu et al., 2006).  
343 ROR2 constructs were expressed by transient transfection in HEK293T cells with the addition of  
344 glycosylation inhibitor kifunensine (Chang et al., 2007). Proteins were isolated from dialyzed  
345 conditioned medium via immobilized metal-affinity chromatography and further purified via size  
346 exclusion chromatography (SEC) in a buffer containing 10 mM HEPES pH 7.5, 150 mM NaCl.

347  
348 **Crystallization and data collection.** Prior to crystallization trials, ROR2 CRD-Kr was concentrated  
349 via ultrafiltration to a final concentration of 25 mg mL<sup>-1</sup> and deglycosylated using a catalytic  
350 quantities of endoglycosidase F1 (Chang et al., 2007) (0.2 μL/50 μL protein solution). Nanolitre-  
351 scale crystallization trials were performed using a Cartesian Technologies robot (100 nL protein  
352 plus 100 nL reservoir solution) in 96-well Greiner plates (Walter et al., 2005). ROR2 CRD-Kr  
353 crystallized in 0.1 M HEPES pH 7.5, 1.5 M LiSO<sub>4</sub> at a temperature of 25°C. Diffraction data were  
354 collected at a temperature of 100 K with crystals mounted within a liquid N<sub>2</sub> cryo-stream. Crystals  
355 were treated with 20% (v/v) glycerol supplemented with reservoir solution and flash-cooled in  
356 liquid N<sub>2</sub> prior to data collection. For Pt-SAD experiments, ROR2 CRD-Kr crystals were soaked in  
357 0.1 M HEPES pH 7.5, 1.5 M LiSO<sub>4</sub> saturated with KPtCl<sub>6</sub> for 1 hour at 25°C prior to cryoprotection  
358 and harvesting. Data were collected using the rotation method. Diffraction data were scaled and  
359 merged using the XIA2 suite (Evans, 2006, Kabsch, 1988, Winter, 2010).

360

361 **Structure solution.** Initial phases for ROR2 CRD-Kr were obtained using Phenix Autosol with Pt-  
362 SAD data (Terwilliger et al., 2009). Four strong Pt sites were identified from substructure solution,  
363 and automated model building of the resultant electron density map was performed using the  
364 program *Buccaneer* (Cowtan, 2006). This produced an interpretable model for the CRD (residues  
365 174-307), but phases were not of a high enough quality to properly trace the Kringle domain  
366 (residues 308-396). Subsequently, the CRD model generated was utilised as a molecular  
367 replacement search model in *Phaser* (McCoy et al., 2007) against higher resolution native data.  
368 This solution was fixed and a second search using a homology model for the Kringle domain  
369 (generated via Swiss-Model) was performed (Waterhouse et al., 2018). This strategy resulted  
370 higher scores in Phaser (LLG = 424, TFZ = 18.9) than searching for the CRD alone (LLG = 94, TFZ =  
371 9.2), indicative of an improved solution. The model for the ROR2 CRD-Kr was manually built using  
372 COOT (Emsley and Cowtan, 2004) and refined to completion using AutoBUSTER (Smart et al.,  
373 2012).

374  
375 **Structure analysis.** Stereochemistry was assessed using the MolProbity server (Davis et al., 2007).  
376 Superpositions were calculated using *Pymol* (Schrodinger, 2015), which was also used to create  
377 ray-traced protein structure images for figures. Residues involved in interactions were identified  
378 using both the PDBsum and Pisa servers (Krissinel and Henrick, 2007; Laskowski, 2001). The  
379 solvent accessible radius was set to 1.4 Å for the representation of all protein surfaces.  
380 Evolutionary structural analysis of CRDs was performed with *SHP* (Riffel et al., 2002; Stuart et al.,  
381 1979) and *PHYLP* (Felsenstein, 1989) to assemble a phylogenetic tree. The structure-based



382 sequence alignment of ROR2 were generated using *UCSF Chimera* (Pettersen et al., 2004) and  
383 prepared for presentation using *ALINE* (Okabayashi et al., 1991).

384

385 **SEC-MALS.** 100  $\mu$ L protein samples were injected onto an S200 10/30 column (GE Healthcare)  
386 equilibrated in a running buffer of 10 mM HEPES pH 7.5, 150 mM NaCl. For analysis of ROR2  
387 oligomeric state, ROR2 ECD was injected at a concentration of 48  $\mu$ M. A Wyatt Dawn HELEOS-II  
388 multi-angle light scattering (MALS) detector and Wyatt Optilab rEX refractive index monitor  
389 recorded both the refractive index and light scattering once separated via SEC. ASTRA software  
390 (Wyatt Technology) was utilized in data analysis.

391

392 **Small-angle X-ray scattering (SAXS).**

393 SAXS experiments were carried out on beamline B21, Diamond Light Source, UK at 25°C, over a  
394 momentum transfer ( $q$ ) range of  $0.01 \text{ \AA}^{-1} < q < 0.45 \text{ \AA}^{-1}$ , where  $q = 4\pi \sin(\theta)/\lambda$ , and  $2\theta$  is the  
395 scattering angle. The ROR2 ECD was injected at onto an inline Shodex KW-402.5 SEC column at a  
396 concentration of 8 mg/mL, in a running buffer of 10 mM Tris pH 7.5, 150 mM NaCl, 1mM  $\text{KNO}_3$ .  
397 Data were collected with a beam energy of 12.4 keV using a Pilatus P3-2M detector. Data  
398 processing and reduction was performed using the program Scatter. Missing residues were  
399 added using Modeller (Eswar et al., 2003) and all-atom ensembles generated using Allosmod  
400 (Weinkam et al., 2012). In each case 50 independent ensembles of 100 models were created.  
401 Calculation and fitting of theoretical scattering curves to collected data was performed by FoXS  
402 (Schneidman-Duhovny et al., 2010). This procedure was automated via the use of Allosmod-FoXS  
403 (Guttman et al., 2013). Flexible models and were then generated using MultiFoXS (Schneidman-

404 Duhovny et al., 2016), as well as relative populations contributing to the overall scatter. This  
405 process produced 10000 conformations from the best-scoring model output from Allosmod,  
406 followed by scoring multi-state models fit to experimental scattering data as described above.

407

#### 408 **Mice**

409 *Ror1/2* double conditional KO mice were generated as previously described (Ho et al., 2012).

410

#### 411 **Cell lines**

412 HEK293T (CRL-3216, ATCC, Manassas, VA) cells were purchased and not re-authenticated. All cell  
413 lines were cultured at 37 degree C and 5% CO<sub>2</sub> in Dulbecco's 324 Modified Eagles Medium  
414 (MT15017CV, Corning) supplemented with 1x glutamine (25-005-CI, Corning), 1x 325 penicillin-  
415 streptomycin (30-002-CI, Corning) and 10% fetal bovine serum (16000069, Thermo Fisher  
416 Scientific).

417 For the derivation for iMEF reporter cells, primary *Ror1<sup>fl/fl</sup>*; *Ror2<sup>fl/fl</sup>*; *ER-cre* MEFs were  
418 isolated directly from E12.5 mouse embryos as described (Susman et al., 2017). Passage 1 or 2  
419 cultures were then immortalized by electroporating with Cas9/CRISPR constructs targeting the  
420 *Tp53* genes using the Neon Transfection System (Thermo Fisher). Transformants were then  
421 serially passaged for 3-5 generations, or until cells from the untransfected control group have  
422 died off. For 4-hydroxytamoxifen (H7904; Sigma-Aldrich) treatments, cells were treated with  
423 0.25 μM of 4-hydroxytamoxifen the first day and then 0.1 μM of 4-hydroxytamoxifen on the  
424 subsequent 3 days. The 4-hydroxytamoxifen containing media were replenished daily. To  
425 introduce the GFP-Pdzrn3 degradation reporter, a PB (PiggyBac)-GFP-Pdzrn3 plasmid, along with

426 a Super PiggyBac Transposase-expressing plasmid, were electroporated into *Ror1<sup>ff</sup>*; *Ror2<sup>ff</sup>*; *ER-*  
427 *cre* iMEFs and then cultured for 7 days. GFP-positive cells were sorted (MoFlo Astrios Cell Sorter,  
428 Beckman Coulter, 488nm laser) to collect the weakly fluorescent (~lowest 1/3 on the FL scale)  
429 cells.

430

### 431 **DNA constructs**

432 Full-length mouse *Ror2* was amplified from MEF cDNA and subsequently cloned into a modified  
433 pENTR-2B vector using *FseI* and *AscI* sites. *Ror2* truncation mutants, Mini-*Ror2* and Robinow  
434 syndrome mutants were generated through Gibson assembly. Open reading frames in pENTR-2B  
435 constructs were then transferred into pLEX\_307 (a gift from David Root; Plasmid 41392,  
436 Addgene) or a modified pLEX\_307 lentiviral vector (short EF1 pLEX\_307) in which the intron in  
437 the EF1 promoter has been moved, using the Gateway LR Clonase II enzyme mix (11791020,  
438 Thermo Fisher). The open-reading frames in all constructs were verified by Sanger sequencing.

439

### 440 **Lentiviral protein overexpression**

441 Lentiviruses were packaged and produced in HEK293T cells by co-transfection of the lentiviral  
442 vectors with the following packaging plasmids: pRSV-REV, pMD-2-G and pMD-Lg1-pRRE (gifts  
443 from Thomas Vierbuchen). 0.1ml or 0.45ml of the viral supernatants was used to infect *Ror1<sup>ff</sup>*;  
444 *Ror2<sup>ff</sup>*; *ER-cre* iMEFs iMEFs seeded at 50% confluency in 12-well plates (per well) for ~16 hrs.  
445 Following removal of the virus-containing media, cells were cultured for 24 hrs. Infected cells  
446 were then selected with puromycin (0.002 mg/ml) for 3 days. Cells from the viral titer that killed

447 a large proportion of cells (60–90%) were expanded and used for FACS; this ensured that the  
448 multiplicity of infection (MOI) is ~1 for all cell lines used in the experiments.

449

#### 450 **Antibodies**

451 Antibodies against Ror1, Ror2, and Kif26b were described previously (Ho et al., 2012, Susman et  
452 al., 2017). The following antibodies were purchased: rabbit anti-Dvl2 (3216, Cell Signaling);  
453 mouse anti- $\alpha$ -tubulin (clone 371 DM1A, ab7291, Abcam); mouse anti-Flag (M2, F1804, Sigma-  
454 Aldrich). Antibodies against Pdzrn3 were described previously (Konopelski, 2021).

455

#### 456 **Western blotting**

457 Protein lysates for SDS-PAGE and western blotting were prepared in 1x - 2x Laemmli sample  
458 buffer or LDS sample buffer (NP0007, Life Technologies). All protein lysates were heated at 95C  
459 for 10min before SDS-PAGE and western blotting. Quantitative western blotting was performed  
460 using the Sapphire gel Imager (Azure BioSystems) according to the manufacturer's instructions.  
461 Non-saturated protein bands were quantified by using Sapphire gel Imager with the gamma level  
462 set at 1.

463

#### 464 **Recombinant proteins and inhibitors**

465 The following recombinant proteins and drugs were purchased: human/mouse WNT5A (654-WN-  
466 010, R&D Systems); Wnt-C59 (C7641-2s; Cellagen Technology); 4-hydroxytamoxifen (H7904;  
467 Sigma-Aldrich). The F2.A anti-Frizzled antibody was previously described (Pavlovic et al., 2018)

468

## 469 **Flow cytometry-based WNT5A signaling assay**

470 Immortalized MEF cells expressing the GFP-Pdzrn3 reporter were plated at a density of  
471 0.08 million/well in a poly-D-lysine-coated 48-well plate. 12 hr after plating, the cells were  
472 incubated with 10 nM Wnt-C59 and allowed to reach confluency. 72 hr after plating, cells were  
473 stimulated with either WNT5A proteins or an equivalent volume of the control buffer (PBS with  
474 0.1% BSA and 0.5% (w/v) CHAPS) in the presence of 10 nM Wnt-C59 for 6 hr. Cells were then  
475 harvested, resuspended in PBS + 0.5% FBS and analyzed using a flow cytometer (FACScan with a  
476 500 nm laser, Becton Dickinson). Raw data were acquired with CellQuest (Becton Dickinson) and  
477 processed in FlowJoX (FLOWJO). Processing entailed gating out dead cells, calculation of median  
478 fluorescence, percent change of medians, and overlay of histograms. For WNT5A dose-response  
479 experiments (Fig. 3B and 3F), cells were treated with the indicated concentrations of WNT5A for  
480 16 hr. For mutant analysis (Fig. 3E and 4B), cells were treated with 200nM WNT5A for 6 hr. For  
481 anti-Frizzled antibody treatment, the F2.A antibody was added to the cells 2 hrs before the start  
482 of WNT5A stimulation and maintained throughout the experiment.

483

## 484 **Acknowledgements**

485 We thank members of the Siebold and Ho labs for their input and discussions. We thank the staff  
486 of Diamond Light Source UK beamlines I03, I23 and B21 for assistance (MX14744 and MX19946),  
487 and K. El Omari, T. Walter, K. Harlos and D. Staunton for technical support. This work was  
488 supported by a National Institutes of Health grant 1R35GM119574 to Hsin-Yi Henry Ho, and  
489 Cancer Research UK (C20724/A26752) to C.S. S.C.G. was supported by a Wellcome Trust-funded

490 DPhil studentship (099675/Z/12/Z). Additional support from the Wellcome Trust Core Award  
491 Grant Number 203141/Z/16/Z is acknowledged.

492

## 493 **References**

- 494 AFZAL, A. R., RAJAB, A., FENSKE, C. D., OLDRIDGE, M., ELANKO, N., TERNES-PEREIRA, E., TUYSUZ,  
495 B., MURDAY, V. A., PATTON, M. A., WILKIE, A. O. & JEFFERY, S. 2000. Recessive Robinow  
496 syndrome, allelic to dominant brachydactyly type B, is caused by mutation of ROR2. *Nat*  
497 *Genet*, 25, 419-22.
- 498 BAZAN, J. F. & DE SAUVAGE, F. J. 2009. Structural ties between cholesterol transport and  
499 morphogen signaling. *Cell*, 138, 1055-6.
- 500 BUNN, K. J., DANIEL, P., ROSKEN, H. S., O'NEILL, A. C., CAMERON-CHRISTIE, S. R., MORGAN, T.,  
501 BRUNNER, H. G., LAI, A., KUNST, H. P., MARKIE, D. M. & ROBERTSON, S. P. 2015. Mutations  
502 in DVL1 cause an osteosclerotic form of Robinow syndrome. *Am J Hum Genet*, 96, 623-  
503 30.
- 504 BYRNE, E. F. X., SIRCAR, R., MILLER, P. S., HEDGER, G., LUCHETTI, G., NACHTERGAELE, S., TULLY,  
505 M. D., MYDOCK-MCGRANE, L., COVEY, D. F., RAMBO, R. P., SANSOM, M. S. P., NEWSTEAD,  
506 S., ROHATGI, R. & SIEBOLD, C. 2016. Structural basis of Smoothed regulation by its  
507 extracellular domains. *Nature*, 535, 517-522.
- 508 CARRON, C., PASCAL, A., DJIANE, A., BOUCAUT, J. C., SHI, D. L. & UMBHAUER, M. 2003. Frizzled  
509 receptor dimerization is sufficient to activate the Wnt/beta-catenin pathway. *J Cell Sci*,  
510 116, 2541-50.
- 511 CHIN, C. N., SACHS, J. N. & ENGELMAN, D. M. 2005. Transmembrane homodimerization of  
512 receptor-like protein tyrosine phosphatases. *FEBS Lett*, 579, 3855-8.
- 513 DANN, C. E., HSIEH, J. C., RATTNER, A., SHARMA, D., NATHANS, J. & LEAHY, D. J. 2001. Insights  
514 into Wnt binding and signalling from the structures of two Frizzled cysteine-rich domains.  
515 *Nature*, 412, 86-90.
- 516 DECHIARA, T. M., KIMBLE, R. B., POUYMIROU, W. T., ROJAS, J., MASIAKOWSKI, P., VALENZUELA,  
517 D. M. & YANCOPOULOS, G. D. 2000. Ror2, encoding a receptor-like tyrosine kinase, is  
518 required for cartilage and growth plate development. *Nat Genet*, 24, 271-4.
- 519 DEGUCHI, H., TAKEYA, H., GABAZZA, E. C., NISHIOKA, J. & SUZUKI, K. 1997. Prothrombin kringle 1  
520 domain interacts with factor Va during the assembly of prothrombinase complex.  
521 *Biochem J*, 321 ( Pt 3), 729-35.
- 522 DIRAC, A. M. & BERNARDS, R. 2003. Reversal of senescence in mouse fibroblasts through  
523 lentiviral suppression of p53. *J Biol Chem*, 278, 11731-4.
- 524 ESWAR, N., JOHN, B., MIRKOVIC, N., FISER, A., ILYIN, V. A., PIEPER, U., STUART, A. C., MARTI-  
525 RENOM, M. A., MADHUSUDHAN, M. S., YERKOVICH, B. & SALI, A. 2003. Tools for  
526 comparative protein structure modeling and analysis. *Nucleic Acids Res*, 31, 3375-80.
- 527 EVANS, P. 2006. Scaling and assessment of data quality. *Acta Crystallogr D Biol Crystallogr*, 62,  
528 72-82.

- 529 GREEN, J. L., KUNTZ, S. G. & STERNBERG, P. W. 2008. Ror receptor tyrosine kinases: orphans no  
530 more. *Trends Cell Biol*, 18, 536-44.
- 531 GRUMOLATO, L., LIU, G., MONG, P., MUDBHARY, R., BISWAS, R., ARROYAVE, R., VIJAYAKUMAR,  
532 S., ECONOMIDES, A. N. & AARONSON, S. A. 2010. Canonical and noncanonical Wnts use a  
533 common mechanism to activate completely unrelated coreceptors. *Genes Dev*, 24, 2517-  
534 30.
- 535 GUTTMAN, M., WEINKAM, P., SALI, A. & LEE, K. K. 2013. All-atom ensemble modeling to analyze  
536 small-angle x-ray scattering of glycosylated proteins. *Structure*, 21, 321-31.
- 537 HO, H. Y., SUSMAN, M. W., BIKOFF, J. B., RYU, Y. K., JONAS, A. M., HU, L., KURUVILLA, R. &  
538 GREENBERG, M. E. 2012. Wnt5a-Ror-Dishevelled signaling constitutes a core  
539 developmental pathway that controls tissue morphogenesis. *Proc Natl Acad Sci U S A*,  
540 109, 4044-51.
- 541 JANDA, C. Y. & GARCIA, K. C. 2015. Wnt acylation and its functional implication in Wnt signalling  
542 regulation. *Biochem Soc Trans*, 43, 211-6.
- 543 JANDA, C. Y., WAGHRAY, D., LEVIN, A. M., THOMAS, C. & GARCIA, K. C. 2012. Structural basis of  
544 Wnt recognition by Frizzled. *Science*, 337, 59-64.
- 545 KABSCH, W. 1988. Automatic indexing of rotation diffraction patterns. *J. Appl. Cryst.*, 21, 67-72.
- 546 KIM, C. & FORRESTER, W. C. 2003. Functional analysis of the domains of the C elegans Ror  
547 receptor tyrosine kinase CAM-1. *Dev Biol*, 264, 376-90.
- 548 KONOPELSKI, S. E., SUSMAN MW, KUNZ R, TAN J, COHEN MD, OKADA K, LAMB H, CHOI SC,  
549 KARUNA EP, SCALES MK, GYGI SP, GREENBERG ME, HO HH. 2021. Proteomic analysis  
550 identifies the E3 ubiquitin ligase Pdzn3 as a regulatory target of Wnt5a-Ror signaling.  
551 *Proc Natl Acad Sci U S A*, 118, e2104944118.
- 552 MEHAWAJ, C., CHOUERY, E., MAALOUF, D., BAUJAT, G., LE MERRER, M., CORMIER-DAIRE, V. &  
553 MEGARBANE, A. 2012. Identification of a novel causative mutation in the ROR2 gene in a  
554 Lebanese family with a mild form of recessive Robinow syndrome. *Eur J Med Genet*, 55,  
555 103-8.
- 556 MIKELS, A., MINAMI, Y. & NUSSE, R. 2009. Ror2 receptor requires tyrosine kinase activity to  
557 mediate Wnt5A signaling. *J Biol Chem*, 284, 30167-76.
- 558 MIKELS, A. J. & NUSSE, R. 2006. Purified Wnt5a protein activates or inhibits beta-catenin-TCF  
559 signaling depending on receptor context. *PLoS Biol*, 4, e115.
- 560 MINAMI, Y., OISHI, I., ENDO, M. & NISHITA, M. 2010. Ror-family receptor tyrosine kinases in  
561 noncanonical Wnt signaling: their implications in developmental morphogenesis and  
562 human diseases. *Dev Dyn*, 239, 1-15.
- 563 MOON, R. T., CAMPBELL, R. M., CHRISTIAN, J. L., MCGREW, L. L., SHIH, J. & FRASER, S. 1993. Xwnt-  
564 5A: a maternal Wnt that affects morphogenetic movements after overexpression in  
565 embryos of *Xenopus laevis*. *Development*, 119, 97-111.
- 566 NACHTERGAELE, S., WHALEN, D. M., MYDOCK, L. K., ZHAO, Z., MALINAUSKAS, T., KRISHNAN, K.,  
567 INGHAM, P. W., COVEY, D. F., SIEBOLD, C. & ROHATGI, R. 2013. Structure and function of  
568 the Smoothed extracellular domain in vertebrate Hedgehog signaling. *Elife*, 2, e01340.
- 569 NAGASAKI, K., NISHIMURA, G., KIKUCHI, T., NYUZUKI, H., SASAKI, S., OGAWA, Y. & SAITOH, A.  
570 2018. Nonsense mutations in FZD2 cause autosomal-dominant omodysplasia: Robinow  
571 syndrome-like phenotypes. *Am J Med Genet A*, 176, 739-742.



- 572 NILE, A. H., MUKUND, S., STANGER, K., WANG, W. & HANNOUSH, R. N. 2017. Unsaturated fatty  
573 acyl recognition by Frizzled receptors mediates dimerization upon Wnt ligand binding.  
574 *Proc Natl Acad Sci U S A*, 114, 4147-4152.
- 575 OISHI, I., SUZUKI, H., ONISHI, N., TAKADA, R., KANI, S., OHKAWARA, B., KOSHIDA, I., SUZUKI, K.,  
576 YAMADA, G., SCHWABE, G. C., MUNDLOS, S., SHIBUYA, H., TAKADA, S. & MINAMI, Y. 2003.  
577 The receptor tyrosine kinase Ror2 is involved in non-canonical Wnt5a/JNK signalling  
578 pathway. *Genes Cells*, 8, 645-54.
- 579 OKABAYASHI, K., NAKAGAWA, Y., HAYASUKE, N., OHI, H., MIURA, M., ISHIDA, Y., SHIMIZU, M.,  
580 MURAKAMI, K., HIRABAYASHI, K., MINAMINO, H. & ET AL. 1991. Secretory expression of  
581 the human serum albumin gene in the yeast, *Saccharomyces cerevisiae*. *J Biochem*, 110,  
582 103-10.
- 583 OLDRIDGE, M., FORTUNA, A. M., MARINGA, M., PROPPING, P., MANSOUR, S., POLLITT, C.,  
584 DECHIARA, T. M., KIMBLE, R. B., VALENZUELA, D. M., YANCOPOULOS, G. D. & WILKIE, A.  
585 O. 2000. Dominant mutations in ROR2, encoding an orphan receptor tyrosine kinase,  
586 cause brachydactyly type B. *Nat Genet*, 24, 275-8.
- 587 PAVLOVIC, Z., ADAMS, J. J., BLAZER, L. L., GAKHAL, A. K., JARVIK, N., STEINHART, Z., ROBITAILLE,  
588 M., MASCALL, K., PAN, J., ANGERS, S., MOFFAT, J. & SIDHU, S. S. 2018. A synthetic anti-  
589 Frizzled antibody engineered for broadened specificity exhibits enhanced anti-tumor  
590 properties. *MAbs*, 10, 1157-1167.
- 591 PERSON, A. D., BEIRAGHI, S., SIEBEN, C. M., HERMANSON, S., NEUMANN, A. N., ROBU, M. E.,  
592 SCHLEIFFARTH, J. R., BILLINGTON, C. J., JR., VAN BOKHOVEN, H., HOOGEBOOM, J. M.,  
593 MAZZEU, J. F., PETRYK, A., SCHIMMENTI, L. A., BRUNNER, H. G., EKKER, S. C. & LOHR, J. L.  
594 2010. WNT5A mutations in patients with autosomal dominant Robinow syndrome. *Dev*  
595 *Dyn*, 239, 327-37.
- 596 REBAGAY, G., YAN, S., LIU, C. & CHEUNG, N. K. 2012. ROR1 and ROR2 in Human Malignancies:  
597 Potentials for Targeted Therapy. *Front Oncol*, 2, 34.
- 598 SALDANHA, J., SINGH, J. & MAHADEVAN, D. 1998. Identification of a Frizzled-like cysteine rich  
599 domain in the extracellular region of developmental receptor tyrosine kinases. *Protein*  
600 *Sci*, 7, 1632-5.
- 601 SATO, A., YAMAMOTO, H., SAKANE, H., KOYAMA, H. & KIKUCHI, A. 2010. Wnt5a regulates distinct  
602 signalling pathways by binding to Frizzled2. *EMBO J*, 29, 41-54.
- 603 SCHNEIDMAN-DUHOVNY, D., HAMMEL, M. & SALI, A. 2010. FoXS: a web server for rapid  
604 computation and fitting of SAXS profiles. *Nucleic Acids Res*, 38, W540-4.
- 605 SCHNEIDMAN-DUHOVNY, D., HAMMEL, M., TAINER, J. A. & SALI, A. 2016. FoXS, FoXSDock and  
606 MultiFoXS: Single-state and multi-state structural modeling of proteins and their  
607 complexes based on SAXS profiles. *Nucleic Acids Res*, 44, W424-9.
- 608 SCHWABE, G. C., TINSCHERT, S., BUSCHOW, C., MEINECKE, P., WOLFF, G., GILLESSEN-KAESBACH,  
609 G., OLDRIDGE, M., WILKIE, A. O., KOMEK, R. & MUNDLOS, S. 2000. Distinct mutations in  
610 the receptor tyrosine kinase gene ROR2 cause brachydactyly type B. *Am J Hum Genet*, 67,  
611 822-31.
- 612 STIEGLER, A. L., BURDEN, S. J. & HUBBARD, S. R. 2009. Crystal structure of the frizzled-like  
613 cysteine-rich domain of the receptor tyrosine kinase MuSK. *J Mol Biol*, 393, 1-9.
- 614 SUSMAN, M. W., KARUNA, E. P., KUNZ, R. C., GUJRAL, T. S., CANTU, A. V., CHOI, S. S., JONG, B. Y.,  
615 OKADA, K., SCALES, M. K., HUM, J., HU, L. S., KIRSCHNER, M. W., NISHINAKAMURA, R.,



- 616 YAMADA, S., LAIRD, D. J., JAO, L. E., GYGI, S. P., GREENBERG, M. E. & HO, H. H. 2017.  
617 Kinesin superfamily protein Kif26b links Wnt5a-Ror signaling to the control of cell and  
618 tissue behaviors in vertebrates. *Elife*, 6.
- 619 TAMHANKAR, P. M., VASUDEVAN, L., KONDURKAR, S., YASHASWINI, K., AGARWALLA, S. K., NAIR,  
620 M., RAMKUMAR, T. V., CHAUBAL, N. & CHENNURI, V. S. 2014. Identification of novel ROR2  
621 gene mutations in Indian children with Robinow syndrome. *J Clin Res Pediatr Endocrinol*,  
622 6, 79-83.
- 623 TUFAN, F., CEFLE, K., TURKMEN, S., TURKMEN, A., ZORBA, U., DURSUN, M., OZTURK, S.,  
624 PALANDUZ, S., ECDER, T., MUNDLOS, S. & HORN, D. 2005. Clinical and molecular  
625 characterization of two adults with autosomal recessive Robinow syndrome. *Am J Med*  
626 *Genet A*, 136, 185-9.
- 627 ULTSCH, M., LOKKER, N. A., GODOWSKI, P. J. & DE VOS, A. M. 1998. Crystal structure of the NK1  
628 fragment of human hepatocyte growth factor at 2.0 Å resolution. *Structure*, 6, 1383-93.
- 629 VAN BOKHOVEN, H., CELLI, J., KAYSERILI, H., VAN BEUSEKOM, E., BALCI, S., BRUSSEL, W., SKOVBY,  
630 F., KERR, B., PERCIN, E. F., AKARSU, N. & BRUNNER, H. G. 2000. Mutation of the gene  
631 encoding the ROR2 tyrosine kinase causes autosomal recessive Robinow syndrome. *Nat*  
632 *Genet*, 25, 423-6.
- 633 VEEMAN, M. T., AXELROD, J. D. & MOON, R. T. 2003. A second canon. Functions and mechanisms  
634 of beta-catenin-independent Wnt signaling. *Dev Cell*, 5, 367-77.
- 635 WATERHOUSE, A., BERTONI, M., BIENERT, S., STUDER, G., TAURIELLO, G., GUMIENNY, R., HEER,  
636 F. T., DE BEER, T. A. P., REMPFER, C., BORDOLI, L., LEPORE, R. & SCHWEDE, T. 2018. SWISS-  
637 MODEL: homology modelling of protein structures and complexes. *Nucleic Acids Res*, 46,  
638 W296-W303.
- 639 WEINKAM, P., PONS, J. & SALI, A. 2012. Structure-based model of allostery predicts coupling  
640 between distant sites. *Proc Natl Acad Sci U S A*, 109, 4875-80.
- 641 WHITE, J., MAZZEU, J. F., HOISCHEN, A., JHANGIANI, S. N., GAMBIN, T., ALCINO, M. C., PENNEY,  
642 S., SARAIVA, J. M., HOVE, H., SKOVBY, F., KAYSERILI, H., ESTRELLA, E., VULTO-VAN  
643 SILFHOUT, A. T., STEEHOUWER, M., MUZNY, D. M., SUTTON, V. R., GIBBS, R. A., BAYLOR-  
644 HOPKINS CENTER FOR MENDELIAN, G., LUPSKI, J. R., BRUNNER, H. G., VAN BON, B. W. &  
645 CARVALHO, C. M. 2015. DVL1 frameshift mutations clustering in the penultimate exon  
646 cause autosomal-dominant Robinow syndrome. *Am J Hum Genet*, 96, 612-22.
- 647 WHITE, J. J., MAZZEU, J. F., COBAN-AKDEMIR, Z., BAYRAM, Y., BAHRAMBEIGI, V., HOISCHEN, A.,  
648 VAN BON, B. W. M., GEZDIRICI, A., GULEC, E. Y., RAMOND, F., TOURAINE, R., THEVENON,  
649 J., SHINAWI, M., BEAVER, E., HEELEY, J., HOOVER-FONG, J., DURMAZ, C. D., KARABULUT,  
650 H. G., MARZIOGLU-OZDEMIR, E., CAYIR, A., DUZ, M. B., SEVEN, M., PRICE, S., FERREIRA, B.  
651 M., VIANNA-MORGANTE, A. M., ELLARD, S., PARRISH, A., STALS, K., FLORES-DABOUB, J.,  
652 JHANGIANI, S. N., GIBBS, R. A., BAYLOR-HOPKINS CENTER FOR MENDELIAN, G., BRUNNER,  
653 H. G., SUTTON, V. R., LUPSKI, J. R. & CARVALHO, C. M. B. 2018. WNT Signaling  
654 Perturbations Underlie the Genetic Heterogeneity of Robinow Syndrome. *Am J Hum*  
655 *Genet*, 102, 27-43.
- 656 WHITE, J. J., MAZZEU, J. F., HOISCHEN, A., BAYRAM, Y., WITHERS, M., GEZDIRICI, A., KIMONIS, V.,  
657 STEEHOUWER, M., JHANGIANI, S. N., MUZNY, D. M., GIBBS, R. A., BAYLOR-HOPKINS  
658 CENTER FOR MENDELIAN, G., VAN BON, B. W. M., SUTTON, V. R., LUPSKI, J. R., BRUNNER,

659 H. G. & CARVALHO, C. M. B. 2016. DVL3 Alleles Resulting in a -1 Frameshift of the Last  
660 Exon Mediate Autosomal-Dominant Robinow Syndrome. *Am J Hum Genet*, 98, 553-561.  
661 WINTER, G. 2010. xia2: an expert system for macromolecular crystallography data reduction. *J.*  
662 *Appl. Cryst.*, 43, 186-190.  
663 XU, Y. K. & NUSSE, R. 1998. The Frizzled CRD domain is conserved in diverse proteins including  
664 several receptor tyrosine kinases. *Curr Biol*, 8, R405-6.  
665 ZEBISCH, M., JACKSON, V. A., ZHAO, Y. & JONES, E. Y. 2016. Structure of the Dual-Mode Wnt  
666 Regulator Kremen1 and Insight into Ternary Complex Formation with LRP6 and Dickkopf.  
667 *Structure*, 24, 1599-605.  
668

669

## 670 **Figure Legends**

671 **Figure 1. Structure of the ROR2 CRD and Kringle domains. A)** Domain layout of ROR2 and  
672 constructs used in this study. **B)** Cartoon representation of the ROR2 CRD-Kr structural unit  
673 coloured in a rainbow representation (N terminus: blue, C terminus:red), with secondary  
674 structural elements indicated and disulfide bonds numbered using Roman numerals. The right  
675 panel shows a 2-domain representation of ROR2, with the CRD in salmon and the Kringle domain  
676 in blue. **C)** Close-up view on the ROR2 CRD-Kr interface rotated 90° relative to **B**. Interface  
677 residues are shown in stick representation and colour-coded as in **B**, right panel. A single  
678 hydrogen bond is displayed as a dashed line. **D)** Structural phylogenetic analysis of CRDs, adapted  
679 from (Nachtergaele et al., 2013) to include ROR2.

680

681 **Figure 2. Comparison of the ROR2 CRD to other Fz-type CRDs. A-D)** CRDs are shown as surface  
682 representation and coloured according hydrophobicity (green: hydrophobic to  
683 white:hydrophilic). Displayed structures: **A)** Fz8-PAM (palmitoleate) complex (PDB 4FOA) (Janda  
684 et al., 2012), **B)** Fz-apo (PDB 1IJY) (Dann et al., 2001), **C)** Smoothened-CLR (cholesterol) complex  
685 (PDB 5L7D) (Byrne et al., 2016) and **D)** ROR2 (from this study). **E-F)** Structural comparison of the

686 CRDs from ROR2 (salmon) and Fz8 (green). A structure-based sequence alignment (E)  
687 corresponding structural superposition (F) are shown. Regions of Wnt8 observed to interact with  
688 Fz8 are displayed in purple. G) Analysis of the “Site 1”-interacting region. The Wnt8 lipid thumb  
689 is shown in purple, with the covalently-attached palmitoleate moiety (PAM) as white sticks. The  
690 lipid-binding groove of Fz8 is displayed as a transparent green surface. A dashed arrow indicates  
691 the required movement of ROR2 helix  $\alpha 5$  in order to prevent a steric clash with the Wnt8 lipid  
692 thumb.

693  
694 **Figure S1. ROR2 purification, characterization and structure solution.** A) Western blot analysis  
695 of the secretion of soluble ROR2 constructs from HEK293T cells. Deletion of the Kringle domain  
696 impairs secretion. B) SEC-MALS analysis of the ROR2 ECD at 2 mg mL<sup>-1</sup> (48  $\mu$ M). The ROR2 ECD  
697 elutes as a monomeric species with a molecular weight of 45.4 kDa. C) Purity assessment by SDS-  
698 PAGE of ROR2 ECD construct purified via IMAC and SEC. D) Structure solution of ROR2 Fz-Kr using  
699 MR-SAD. Pt-soaked crystals enabled the determination of a model for the Fz-CRD using *Phenix*  
700 *Autosol* (yellow, left). The Kringle domain could not be built without an MR search using an  
701 ensemble of homology models generated using *Rosetta*. The final structure was refined using  
702 *AutoBUSTER* (salmon/blue, right). E) Identification of sulfur sites in ROR2 Fz-Kr using long-  
703 wavelength data collection at I23. A total of 8 disulfide bonds (I-VIII) could be resolved, as well as  
704 4 methionine side chains (Met-1 to Met-4) and 2 sulphate ions. F) Disulfide bond VI is in a flexible  
705 region between the two domains, but is accounted for in the anomalous map. Anomalous  
706 difference density is contoured at 3 $\sigma$  (yellow) and 2Fo-Fc density at 1 $\sigma$  (blue).

707

708 **Figure S2. SAXS solution structure of the ROR2 ECD. A)** Experimental scattering curve (black) and  
709 calculated scattering from models (blue), shown to a maximum momentum transfer of  $0.35 \text{ \AA}^{-1}$ .  
710 A fitting residual between the experimental and calculated scattering patterns is displayed. **B)**  
711 Full-length models of the ROR2 ECD and their relative populations contributing to the model  
712 scattering curve, as calculated by Multi-FOXS. **C)** Experimental (black) and calculated (blue)  
713 Guinier region. The shaded area indicates the region used for  $R_g$  analysis. The calculated radius  
714 of gyration ( $R_g$ ) and molecular weight derived from the volume of correlation metric  $V_c$  ( $MW_{Vc}$ )  
715 are displayed. **D)** Normalised pair distance distribution ( $P(r)$ ) function and derived maximum  
716 intra-particle distance distribution function ( $D_{max}$ ).

717

### 718 **Figure 3. Requirement of the ROR2 CRD and Frizzleds in WNT5A signaling**

719 **A)** Workflow of the ROR2 central rescue paradigm. Primary MEF cultures generated from E12.5  
720 *ROR1<sup>fl/fl</sup>; ROR2<sup>fl/fl</sup>; Cre-ER* mouse embryos were immortalized by CRISPR/Cas9-mediated deletion  
721 of the *Tp53* gene. A WNT5A-ROR signaling reporter (GFP-Pdzrn3) was stably inserted in the  
722 immortalized MEFs (iMEFs) via lentiviral transduction. *ROR1/ROR2* conditional mutant iMEFs  
723 were then treated with 4-OHT to activate the Cre-ER recombinase and delete the *ROR1* and *ROR2*  
724 genes. To test the function of mutant ROR2 variants, WT or mutant ROR2 proteins were re-  
725 expressed in *ROR1/ROR2* double KO (ROR DKO) iMEFs via lentiviral transduction. **B)** Dose-  
726 response curves showing WNT5A-ROR signaling activity, as assayed by GFP-Pdzrn3 degradation,  
727 as a function of WNT5A concentration in ROR DKO iMEFs or ROR DKO iMEFs re-expressing WT  
728 ROR2. Each datapoint was calculated from the median fluorescence (after WNT5A stimulation –  
729 before WNT5A stimulation/before WNT5A stimulation) of the GFP-Pdzrn3 reporter from 20,000

730 – 30,000 cells. **C)** Schematic of ROR2 truncation mutants and the mini-ROR2 construct. **D)**  
731 Western blot showing expression of the endogenous ROR2 in the ROR double conditional KO  
732 iMEFs (Lane 1), the abolition of ROR2 expression in ROR DKO iMEFs (Lane 2), the re-expression  
733 of WT (Lane 3) and mutant ROR2 variants (Lanes 4-9). The WT or mutant ROR2 bands are marked  
734 with asterisks for clarity. Tubulin was used as the loading control. **E)** Quantification of the effects  
735 of ROR2 mutant variants in rescuing WNT5A-ROR signaling, as assayed by GFP-Pdzn3  
736 degradation. Error bars represent  $\pm$  SEM calculated from three technical replicates. t-test  
737 (unpaired) was performed to determine statistical significance for mutants vs. WT ROR2 rescue.  
738 **F)** Effects of the anti-Frizzled antibody F2.A on WNT5A signaling, as assayed by GFP-Pdzn3  
739 degradation in ROR DKO iMEFs or ROR DKO iMEFs re-expressing WT ROR2, over a range of  
740 WNT5A doses. Each datapoint was calculated from the median fluorescence (after WNT5A  
741 stimulation – before WNT5A stimulation/before WNT5A stimulation) of the GFP-Pdzn3 reporter  
742 from 20,000 – 30,000 cells. **G)** Model of ROR2 CRD and Frizzled action in WNT5A-ROR signaling.

743

744 **Figure 4. Analysis of Robinow syndrome mutations in the ROR2 CRD and Kr**

745 **A)** Western blot showing expression of WT ROR2 and Robinow syndrome ROR2 mutants in the  
746 ROR DKO iMEF reporter cells. **B)** Quantification of the effects of Robinow syndrome ROR2  
747 mutants in rescuing WNT5A-ROR signaling, as assayed by GFP-Pdzn3 degradation. Error bars  
748 represent  $\pm$  SEM calculated from three technical replicates. t-test (unpaired) was performed to  
749 determine statistical significance for mutants vs. WT ROR2 rescue. **C)** Structure of the ROR2  
750 CRD-Kr tandem domains showing the location of the Robinow syndrome mutations. **D)** Close-

751 up view of C223 and R272. **E)** Close-up view of C182, R184 and R189. **F)** Close-up view of G326  
752 and R366.

## Figure 1

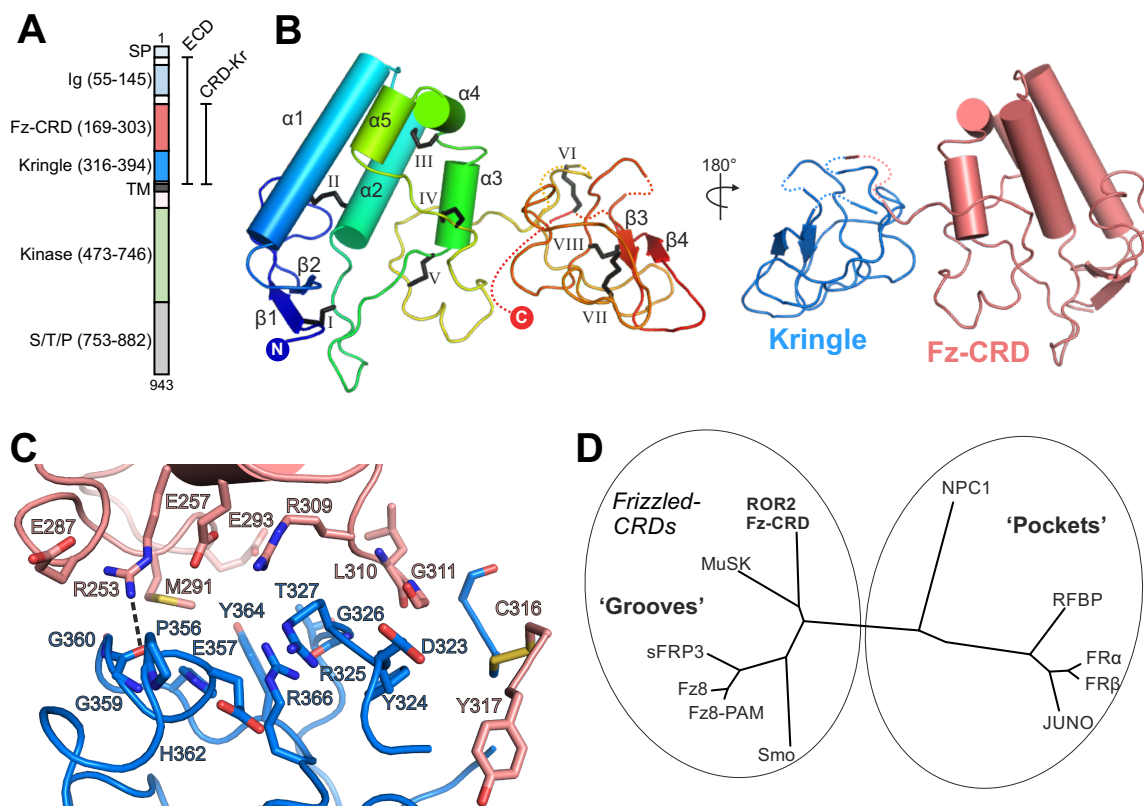


Figure S1

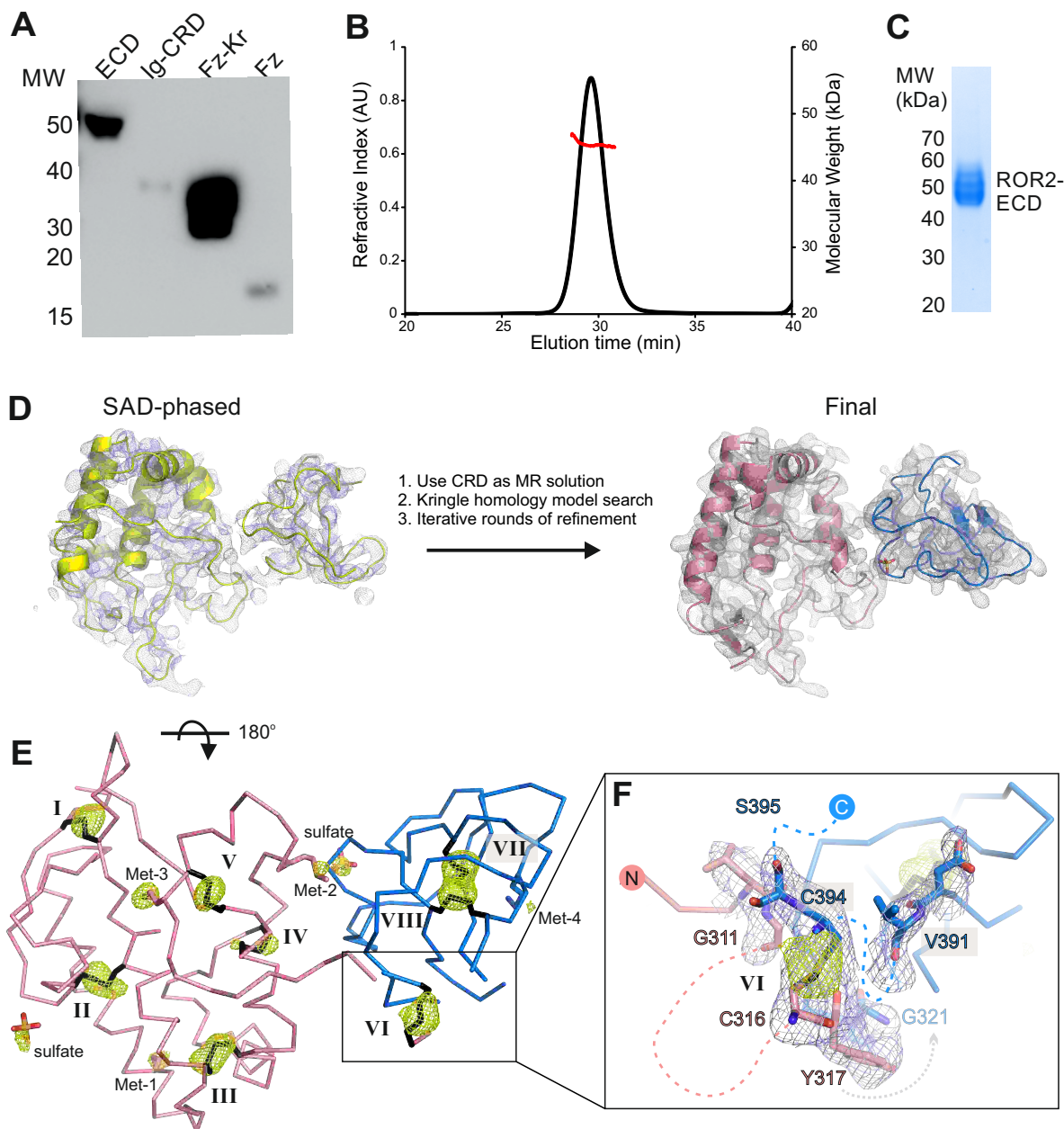




Figure 2

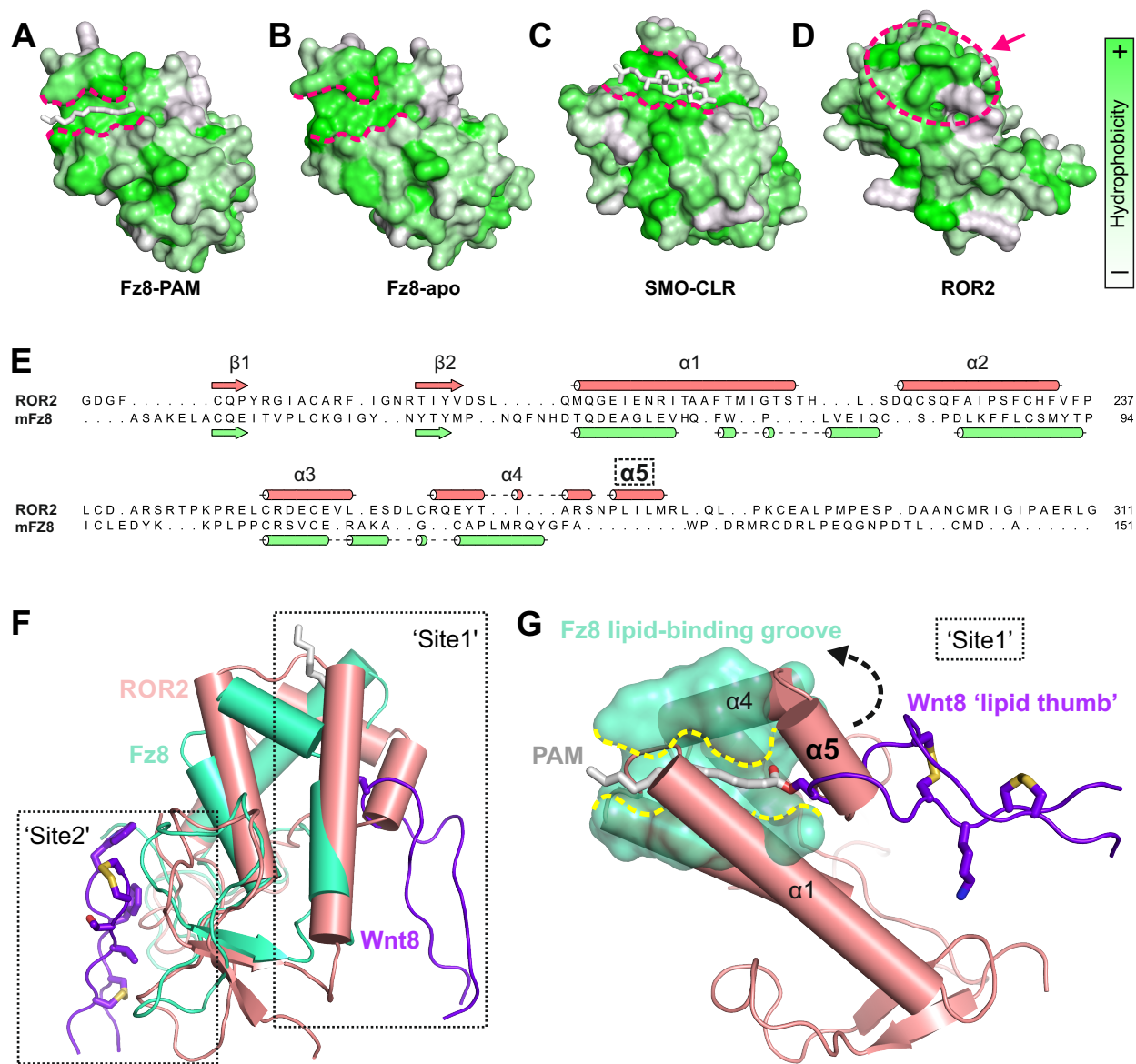
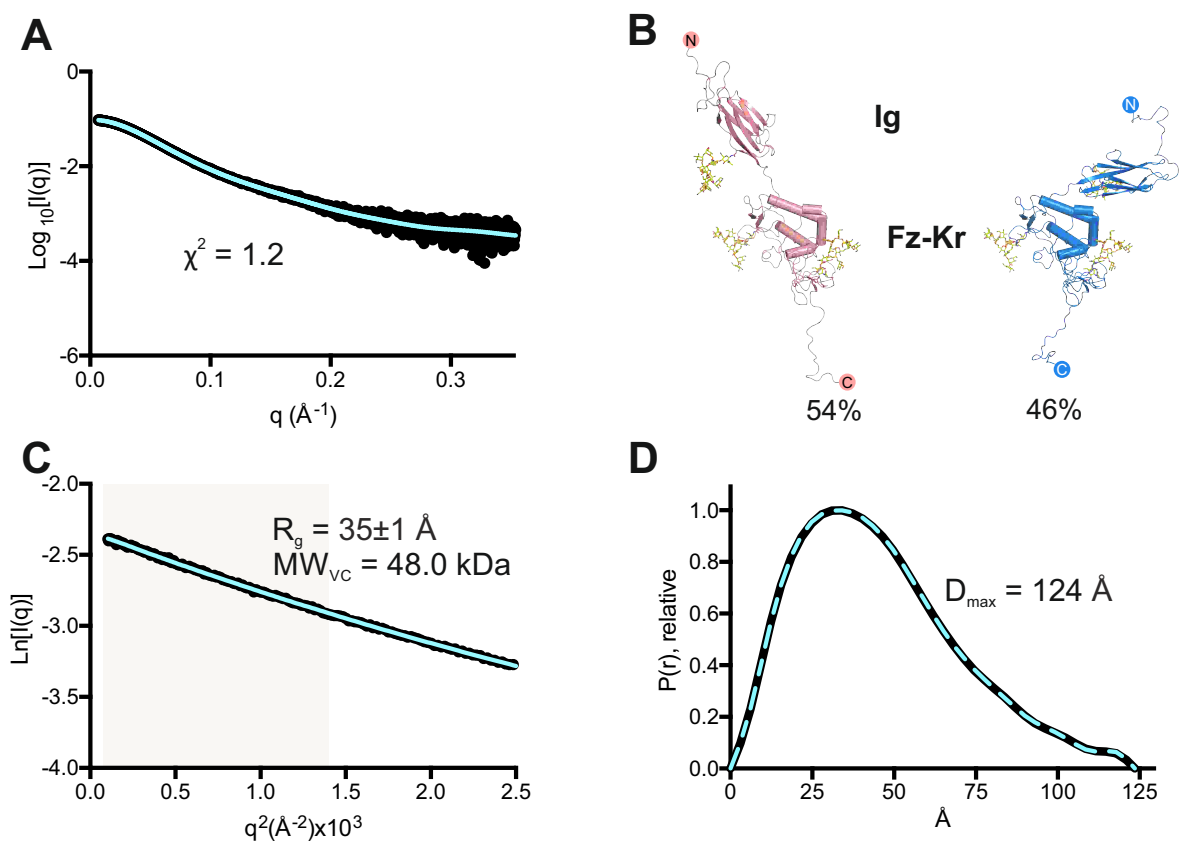


Figure S2



**Figure 3**

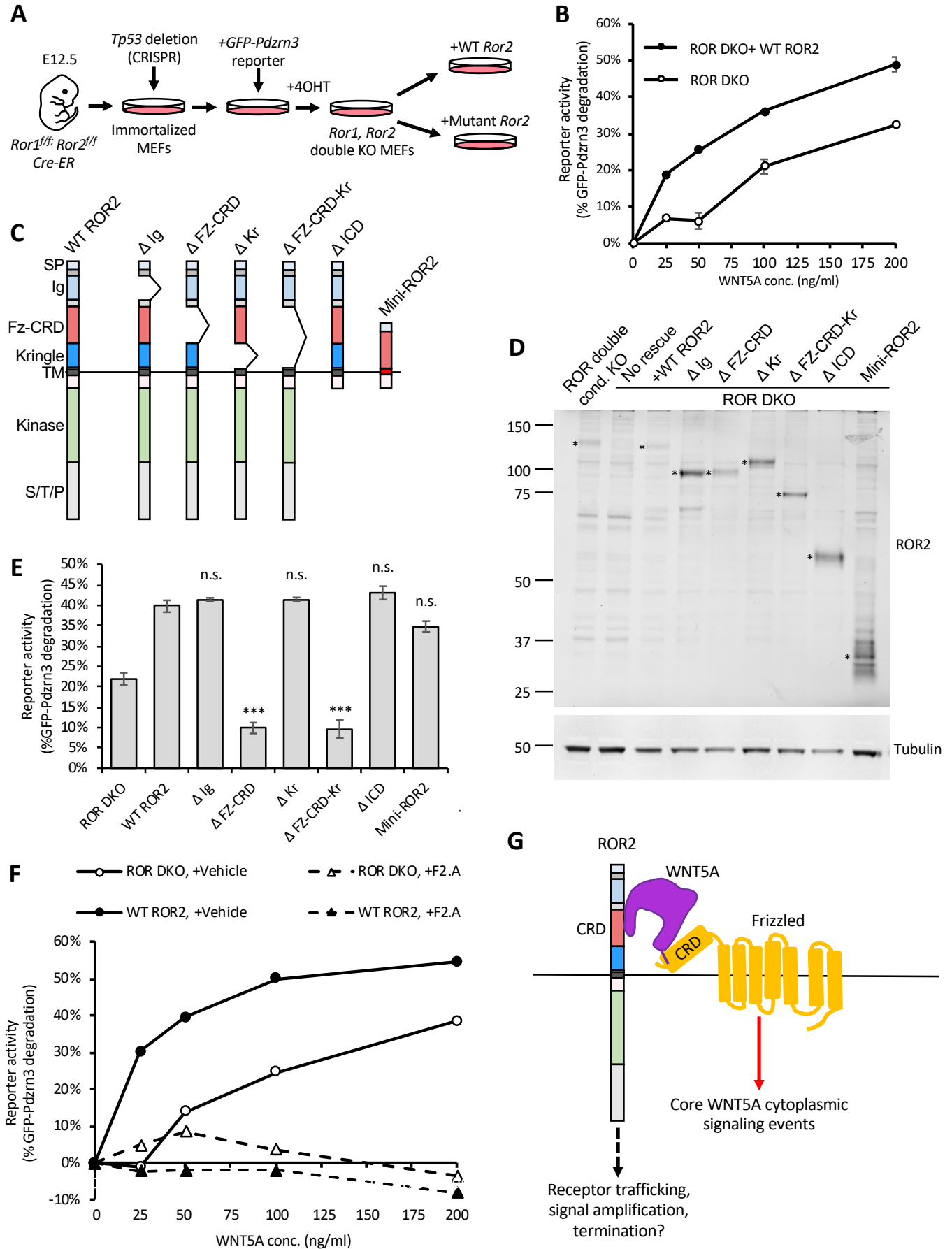


Figure 4

